Science of the Total Environment 892 (2023) 164567

Contents lists available at ScienceDirect

Science of the Total Environment

journal homepage: www.elsevier.com/locate/scitotenv

Identification and contribution of potential sources to atmospheric lead pollution in a typical megacity: Insights from isotope analysis and the Bayesian mixing model

Wen-Jing Dai [a,b], Xiao-Dong Li [a,*], Yu-Cong Fu [c,d], Shi-Yuan Ding [a], Qin-Kai Li [a], Zhi-Qi Zhao [b,*]

[a] School of Earth System Science, Tianjin University, Tianjin 300072, China
[b] School of Earth Science and Resource, Chang'an University, Xi'an 710054, China
[c] State Key Laboratory of Environmental Geochemistry, Institute of Geochemistry, Chinese Academy of Sciences, Guiyang 550081, China
[d] University of Chinese Academy of Sciences, Beijing 100049, China

HIGHLIGHTS

- The elevated Pb concentrations in January relate to coal combustion for heating.
- The PM_{10}-bond Pb mainly originate from local Pb emission sources.
- Main sources of Pb in PM_{10} are coal combustion, vehicle, steel plants emissions.
- The contribution of coal combustion in January exceed 50 % by the MixSIAS model estimated.

GRAPHICAL ABSTRACT

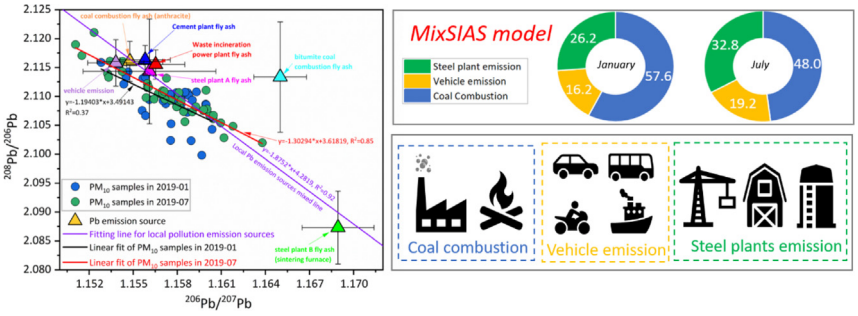

ARTICLE INFO

Editor: Xinbin Feng

Keywords:
PM_{10}
Pb isotopic compositions
MixSIAR model
Source appointment

ABSTRACT

Atmospheric particulate matter (PM) enriched with lead (Pb) has severe irreversible effects on human health. Therefore, identifying the contribution of Pb emission sources is essential for protecting the health of residents. Using the Pb isotopic tracer method, this study explored the seasonal characteristics and primary anthropogenic Pb sources for atmospheric PM in Tianjin in 2019. We calculated the contribution of Pb sources using the end-member and MixSIAR models. The results showed that Pb loaded in PM_{10} was more abundant in January than in July, and was strongly influenced by meteorological conditions and anthropogenic emissions. The primary Pb sources of the aerosol samples originated from coal combustion and vehicle and steel plant emissions, mainly originating from local Pb emission sources in Tianjin. The PM_{10}-bond Pb in January was influenced by regional transportation and local sources. The MixSIAS model calculated the contribution of coal combustion as approximately 50 %. Compared with that in January, the contribution of coal combustion decreased by 9.6 % in July. Our results indicate that some of the benefits of phased-out leaded gasoline have been short-lived, whereas other industrial activities releasing Pb have increased. Furthermore, the results emphasise the practicability of the Pb isotope tracer source approach for identifying and distinguishing between different anthropogenic Pb inputs. Based on this study, scientific and effective air pollution prevention and control programs can be formulated to provide decision support for the guidance and control of air pollutant emissions.

1. Introduction

With the rapid expansion of industrialisation, urbanisation, and agricultural development, the increased demand for nonrenewable energy in

* Corresponding authors.
E-mail addresses: xiaodong.li@tju.edu.cn (X.-D. Li), zhaozhiqi@chd.edu.cn (Z.-Q. Zhao).

http://dx.doi.org/10.1016/j.scitotenv.2023.164567
Received 3 March 2023; Received in revised form 10 May 2023; Accepted 28 May 2023
Available online 1 June 2023

China has led to a severe deterioration of air quality in the Beijing-Tianjin-Hebei (BTH) region, which has increased the concentration of particulate matter (PM) entering the atmosphere. PM, especially PM_{10} (diameter < 10 μm) and $PM_{2.5}$ (diameter < 2.5 μm), are significant pollutants causing air quality degradation in this region (Gao et al., 2015; Huang et al., 2018). PM has a strong adsorption capacity for toxic metal(loid)s. With prolonged exposure to heavy pollution, toxic metal(loid)s can accumulate in the human body because of their non-biodegradability and stability, thereby increasing morbidity and mortality through cardiovascular, lung, and respiratory diseases (Charlesworth et al., 2003; Li et al., 2013; Fang et al., 2017; Wu et al., 2020). Lead (Pb) is an extremely pervasive and toxic trace metal (Marx et al., 2016). The Pb loaded onto PM enters the environment via dry and wet atmospheric deposition (Child et al., 2018; Graney et al., 2019; Gao et al., 2021). The widespread presence of Pb in the environment poses a significant potential risk to human health and the ecological environment and has gained wide public concern (Fry et al., 2020; Harlavan et al., 2021).

Anthropogenic emissions are significant contributors to the total atmospheric Pb emission flux. Anthropogenic sources of Pb emissions are 1.5 times greater than natural emissions (Rauch and Pacyna, 2009). Since the second industrial revolution, global Pb pollution has increased significantly (Marx et al., 2016; Pérez-Rodríguez et al., 2018). After the phase-out of Pb gasoline in 2000, atmospheric Pb emissions in China declined significantly which the total Pb emissions decreased by approximately 81 % (Li et al., 2012); subsequently, Pb emissions again increased rapidly in the following years due to industrial activities (Li et al., 2013; Tian et al., 2015; Wan et al., 2020). Anthropogenic Pb emissions in 2012 reached 14,397.6 t $year^{-1}$. Several studies have shown that the total amount of Pb released into the atmosphere increases in proportion to industrial consumption; however, the detailed rationale for this relationship remains unclear (Li et al., 2019). Therefore, decoding the specific anthropogenic sources and contributions of atmospheric Pb is crucial as well as comprehensively understanding their pollution status and seasonal characteristics to reduce the emission of toxic substances and control exposure risk.

Since the ban on leaded gasoline in China in 2000, rapid industrialisation accompanied by high levels of coal consumption has resulted in fossil fuel combustion and non-ferrous metal smelting, contributing to atmospheric Pb pollution. Thus, industrial emissions gradually replaced vehicle exhaust as the main source of atmospheric Pb pollution (Xu et al., 2017; Li et al., 2019). Because the source of the contaminant Pb could be determined using the Pb isotope tracer method, distinguishing between different industrial sources of Pb was feasible. The isotopic fingerprinting method identifies atmospheric Pb from land-based or anthropogenic sources by comparing the isotopic ratios of Pb in PM samples with those of possible Pb sources (Tao et al., 2021; Chen et al., 2023).

Owing to the complexity and heterogeneity of Pb pollution in urban environments, Pb pollution end-members in cities are often variable. Therefore, better understanding the atmospheric sources and dispersion processes of Pb pollution is important to developing urban environmental protection measures. Several previous studies have used the end-member mixing model to calculate source apportions for environmental samples; however, the originally reported sources have some uncertainty regarding local emission sources (Moore and Semmens, 2008). It is unclear whether another method could consider the uncertainties and quantitative analysis of Pb emission sources could be conducted quickly and easily to quantify the source contributions range. Currently, the MixSIAS model is considered a new and useful model for estimating multiple sources' contributions. The MixSIAS model has been applied to quantify source contributions in several environmental media, such as soil, water, atmospheric PM, and road dust (Dietrich et al., 2021; Hu et al., 2022; Liu and Han, 2021; Chen et al., 2023).

Spatially, most atmospheric heavy metal emissions are concentrated in relatively developed regions in China, such as in the north and east (Tian et al., 2015). Tianjin is a typical urbanised megacity with a highly industrialised and densely populated area. It is the largest port city in northern China, with modern manufacturing and shipping. To quantify the range of source contributions and the potential variation in multiple sources over the seasons, we used the MixSIAS model based on Pb isotopic compositions. The main objectives of our study were: (1) to elucidate the seasonal characteristics of PM_{10} concentrations, Pb isotopic composition, and the Pb isotopic characteristics of local Pb emission sources in Tianjin; (2) to identify the sources of Pb in PM_{10}; and (3) to estimate the range of contribution of local Pb emission sources using the MixSIAS model.

2. Materials and methods

2.1. Sampling

The aerosol sampling site (39.11°N, 117.16°E) was located in the 19th Teaching Building, Weijin Road Campus, Tianjin University, Nankai District, Tianjin, China. The sampler was installed on a rooftop platform at approximately 25 m. The site was situated in a typical urban environment surrounded by arterial roads, residential and commercial areas, schools, and parks. No pollution sources, such as factories or construction sites, were within 10 km of the sampling sites.

According to data from the Second National Pollution Source Census Bulletin, the top three atmospheric PM emissions industries are non-metallic mineral products, coal mining and washing, ferrous metal smelting, and rolling processing, which accounted for 54.77 % of the PM emissions from industrial sources. In this study, the sources of atmospheric PM from coal-fired/waste incineration power plants, iron and steel smelting plants, and cement plants correspond to the power and heating industries, ferrous metal smelting industries, and non-metallic mineral products industries, respectively. In addition, previous studies have reported that atmospheric Pb may originate from traffic sources and biomass combustion (Tao et al., 2021; Kayee et al., 2020). The sources of Pb emissions are summarised in Table S1.

Using a kC-1000 high-flow PM_{10} sampler (Laoshan Application, Qingdao, Shandong, China), 72 PM_{10} samples (excluding two blank filters) were collected on consecutive days in different seasons (winter: from the 7th to the 22nd of January 2019; summer: from 11th to 31st of July 2019) based on the average Air Quality Index (AQI). The samples of clean episodes accounted for approximately 65 % of the total number of PM_{10} samples (setting AQI < 100 represented a clean period, and AQI > 100 represented a contaminated period). Hourly AQI were collected from monitoring data released by the Tianjin Environmental Monitoring Station. Based on the wind roses during the sampling period, the dominant wind directions in winter and summer were northwest and southeast, respectively (Fig. S1). The monthly average meteorological parameters for January and July are listed in Table S2. Meteorological data were obtained from the data released by Tianjin Meteorological Bureau (http://tj.cma.gov.cn/). The sampling flow rate was 1.05 m^3 min^{-1} using a pre-fired quartz fibre filter (200 mm × 250 mm, Laoshan Application, Qingdao, Shandong, China), and the sampling period was 12 h. In particular, the samples were used to determine secondary inorganic ions, including sulphates, nitrates, and ammonium salts (SNA)-related indicators in addition to testing for Pb isotopic compositions; therefore, we used quartz filters to collect PM_{10} samples. Traffic emissions source samples were collected using a diaphragm pump (Laoying 3072, Laoying Environ. Tech., Qingdao, Shandong, China) at a flow rate of 3 L min^{-1}. The flue gas was collected using the American Environmental Protection Agency (EPA) fixed-source flue gas collection method for samples from industrial sources. The Pb-source samples were collected using a Teflon filter (φ20 mm, Pall, USA). The filter was dried for 48 h and weighed on an electronic balance (Mettler Toledo ML204T, Switzerland). After weighing, the filters were placed in sealed polyethylene bags and stored in a refrigerator until analysis. Using the same sampling procedure as that for the aerosol and Pb source samples, blank samples were collected on quartz samplers for the corresponding sampling time for analysis. The samples were

corrected for Pb concentration data. The blanks were deduced from the calculation of the Pb concentrations.

2.2. Sample analysis

In this study, we assessed the impacts of anthropogenic emissions on atmospheric Pb to elucidate the contribution of anthropogenic Pb (unstable) to the total Pb load (Outridge et al., 2002; Gioia et al., 2006; Ewing et al., 2010). We have described this part in more detail in the supplemental material Test S1. Previous studies have used this method to identify and differentiate between anthropogenic and lithospheric Pb in sediments (Peng et al., 2022a, 2022b). For the aerosol samples, Pb was extracted via dilute acid leaching with 5 % HNO_3 (Zhao et al., 2015). Pb source samples were digested with a 6:3:1 mixture of concentrated HF-HCl-HNO_3 in Teflon digestion tanks on a hotplate at 120 °C for 24 h (all acids were double-distilled acids purified using an acid purification system). Pb in the resulting leachate and digestate was separated and purified using Dowex–1 × 8 anion exchange resin (200–400 mesh) micro-exchange column, using the acid of HBr and HCl as the eluent. Additional details regarding the sample separation and purification procedures are listed in Table S3. Before measuring the Pb isotopic composition, the purified samples were dissolved in 5 mL of 2 % (*v*/v) HNO_3 and stored in a refrigerator. All sample pretreatment processes were performed in an ultra-clean laboratory with a high purification level.

The Pb concentration was measured using ICP-MS (NexION 300×, Perkin Elmer, USA) with an analytical precision better than 5 %, using Rhodium as an internal standard. The Pb blank for the entire experimental procedure (<0.1 ng) had an insignificant effect on the Pb isotopic measurements of all samples. The recovery of Pb ranged from 80 % to 110 %, according to the international standard reference material NIST SRM-981, following the same purification procedure. The Pb isotopic composition was determined by MC-ICP-MS (Neptune Plus, Thermo Fisher Scientific, USA) with a 1σ precision of ±0.01 % (Ewing et al., 2010), and Pb isotopic ratios were corrected by the $^{205}Tl/^{203}Tl$ ratio (NIST SRM-3158, internal standard) for the mass fractionation using the exponential fractionation law (Outridge et al., 2002; Widory et al., 2004). Standard reference material NIST-981 with known Pb compositions was subsequently measured after about every 5–10 samples to correct measurement deviation and drift for calibration and quality check. The instrument was optimally adjusted to ensure the best accuracy (consisting of 60 scans) for Pb isotopic compositions (Hinrichs et al., 2002). The measured values of NIST SRM-981 were $^{206}Pb/^{204}Pb$ = 16.9348 ± 0.0011, $^{207}Pb/^{204}Pb$ = 15.4889 ± 0.0012, and $^{208}Pb/^{204}Pb$ = 36.6886 ± 0.0033 (n = 18), which were consistent with the reference values of 16.9322, 15.4855, and 36.6856, respectively (Todt et al., 1993).

2.3. Estimation of contribution from Pb pollution sources

Various chemical and mathematical methods can be used to calculate the contribution of pollution sources, including mass balance, mixing end-members, and Bayesian mixing models. This study used the MixSIAS model based on a Bayesian tracer mixing model combined with the isotope method to estimate the contributions of different anthropogenic Pb emission sources. Compared with traditional mixing models, the MixSIAS model accounts for the variability in pollution sources and mixture tracer data more accurately (Moore and Semmens, 2008). This method also allows assessment of the uncertainty in the source isotopic composition by feeding the standard deviation of the source composition into the model (Dietrich et al., 2021). MixSIAS is a free, open-source R software package. Stock and Semmens (2016)) and Stock et al. (2018) provided complete equations and explanations, relative guidance for source assignment in the mixing system, and applied covariate data to the MixSIAS model. The specific algorithm for the MixSIAS model is summarised in Supplementary Material Test S2. Finally, the percentage contribution of each source was obtained by entering the calculation code in R language with raw data files of the values of $^{206}Pb/^{207}Pb$ and $^{208}Pb/^{206}Pb$ ratios and standard deviations for each source (Fig. 1).

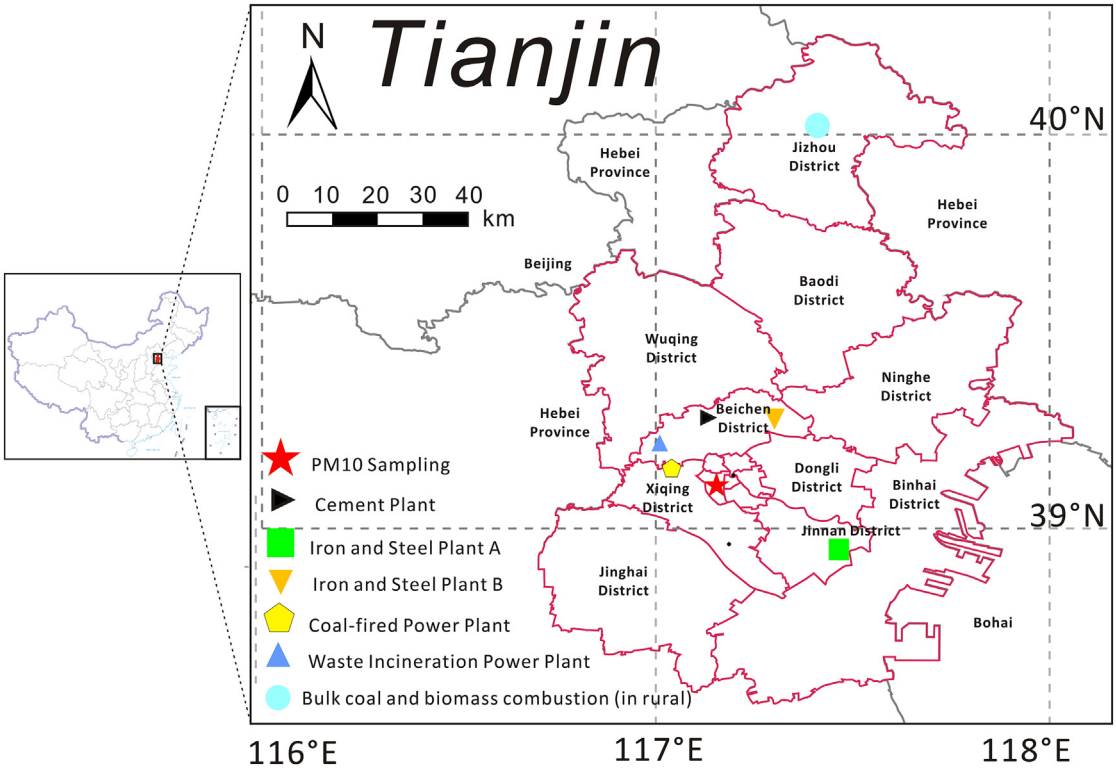

Fig. 1. Map of sampling site in Tianjin, China.

3. Results and discussion

3.1. Temporal variation characteristics of Pb concentration and Pb isotopic compositions in PM_{10} samples

3.1.1. Seasonal variation characteristics of Pb concentration and Pb isotopic ratios

The Pb concentrations and isotopic compositions of the PM_{10} samples measured in this study are shown in Table S4. The average content of Pb in PM_{10} (acid-soluble fraction) reached 13.3 ± 11.2 ng m^{-3} (n = 31) in January, and 7.9 ± 3.8 ng m^{-3} (n = 4) in July. After implementing a policy to entirely phase-out leaded petrol in China in 2000, the Pb concentration in PM_{10} significantly decreased, consistent with the results of many studies (Chen et al., 2005; Chen et al., 2008). However, the Pb content in the PM collected during each period was different, which was inextricably linked to whether the sampling timing coincided with the implementation of national air pollution control policies. Seasonal differences were observed in the average Pb concentration of PM_{10} ($p < 0.01$). The elevated Pb concentrations may be related to increased coal combustion for heating in January, which had a lower temperature. In contrast, a smaller variation in the Pb isotopic ratios was observed in PM_{10}. No significant seasonal difference and diurnal variations were observed in the Pb isotopic composition of PM_{10} ($p > 0.1$) (Fig. 2b, c, e, f), indicating that the final ambient Pb isotopic compositions in the two seasons and diurnal likely had similar sources and/or a similar mix of sources. Notably, the similarity in Pb isotopic ratios does not always imply a similar Pb source as the final Pb may be derived from a mixture of several different sources (Lee et al., 2017).

The variation in Pb concentration in PM_{10} during polluted episodes was significantly higher than that in clean episodes in both seasons. The mean Pb concentrations in January for polluted and clean episodes were 18.5 ± 11.5 (n = 19) and 5.0 ± 2.5 ng m^{-3} (n = 16), respectively. In contrast, the summer Pb concentrations reached 11.1 ± 2.7 (n = 7) and 7.2 ± 3.4 ng m^{-3} (n = 34) in July for polluted and clean episodes, respectively. The distribution ranges of Pb isotopic compositions in the clean episodes were slightly wider (Fig. 2h, i). The $^{206}Pb/^{207}Pb$ ratio and Pb concentrations were lower than those in the polluted episodes, suggesting that a/several relatively high $^{206}Pb/^{207}Pb$ ratio source(s) may have been added or the contribution ratios of the source(s) may have improved during the pollution period.

3.1.2. Diurnal variation characteristics of Pb concentration and Pb isotopic compositions

The time series of the AQI, relative humidity (RH), Pb concentration, and the corresponding $^{206}Pb/^{207}Pb$ ratios in PM_{10} are shown in Fig. 3. The Pb content in PM_{10} and amplitude of the variations were more abundant and significant, respectively, in January than in July (Fig. 3). As shown in Fig. 3, other severe and longer-duration pollution events were present in January (Case 1: from 10th to 13th) and July (Case 2: from 16th to 18th), including a gradual increase in Pb concentrations to a

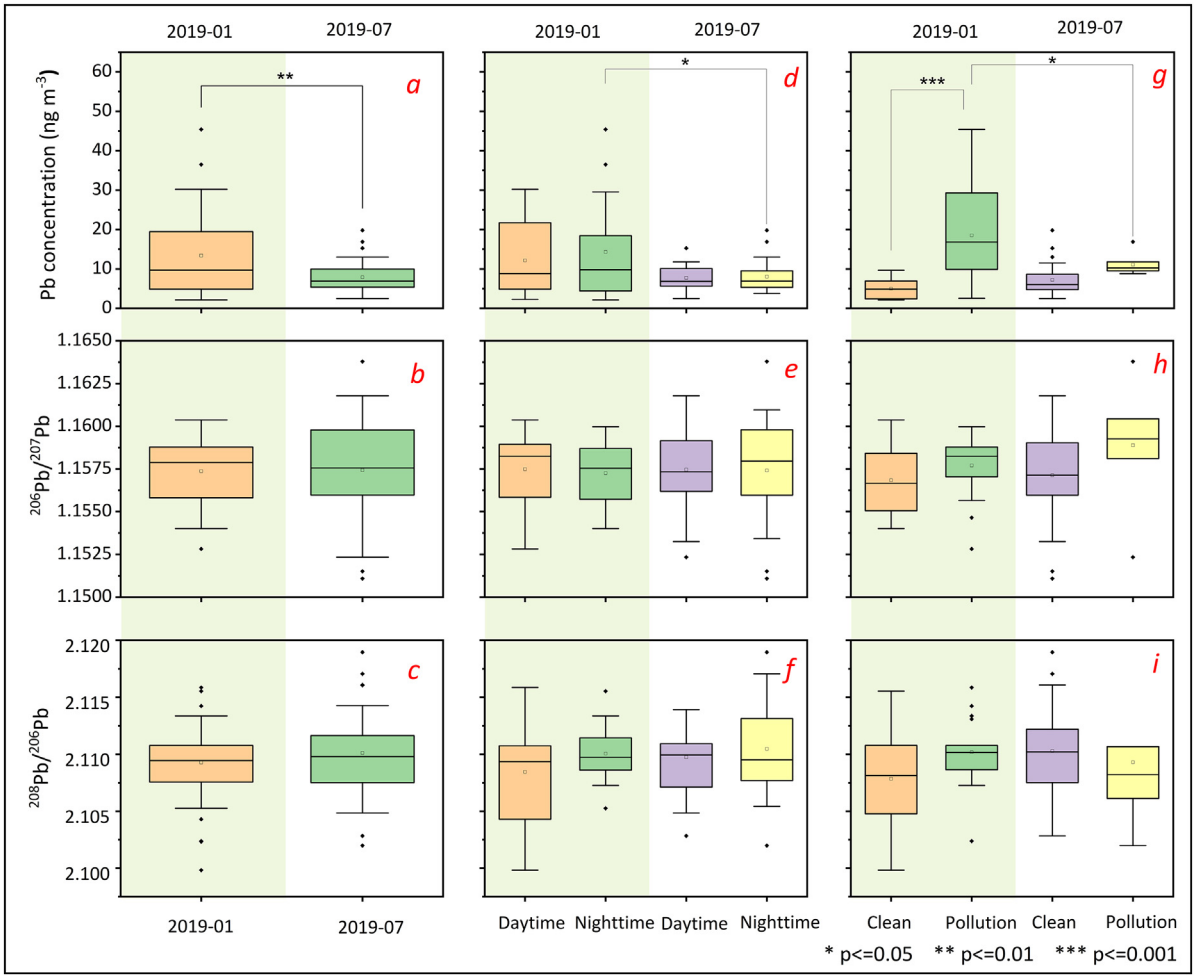

Fig. 2. Seasonal variation of Pb concentration and isotope ratios in PM_{10}. (a, b, c) Pb concentration, $^{206}Pb/^{207}Pb$ ratios, $^{208}Pb/^{206}Pb$ ratios in January and July. (d, e, f) Pb concentration, $^{206}Pb/^{207}Pb$ ratios, $^{208}Pb/^{206}Pb$ ratios in daytime and nighttime. (g, h, i) Pb concentration, $^{206}Pb/^{207}Pb$ ratios, $^{208}Pb/^{206}Pb$ ratios in pollution and clean episodes.

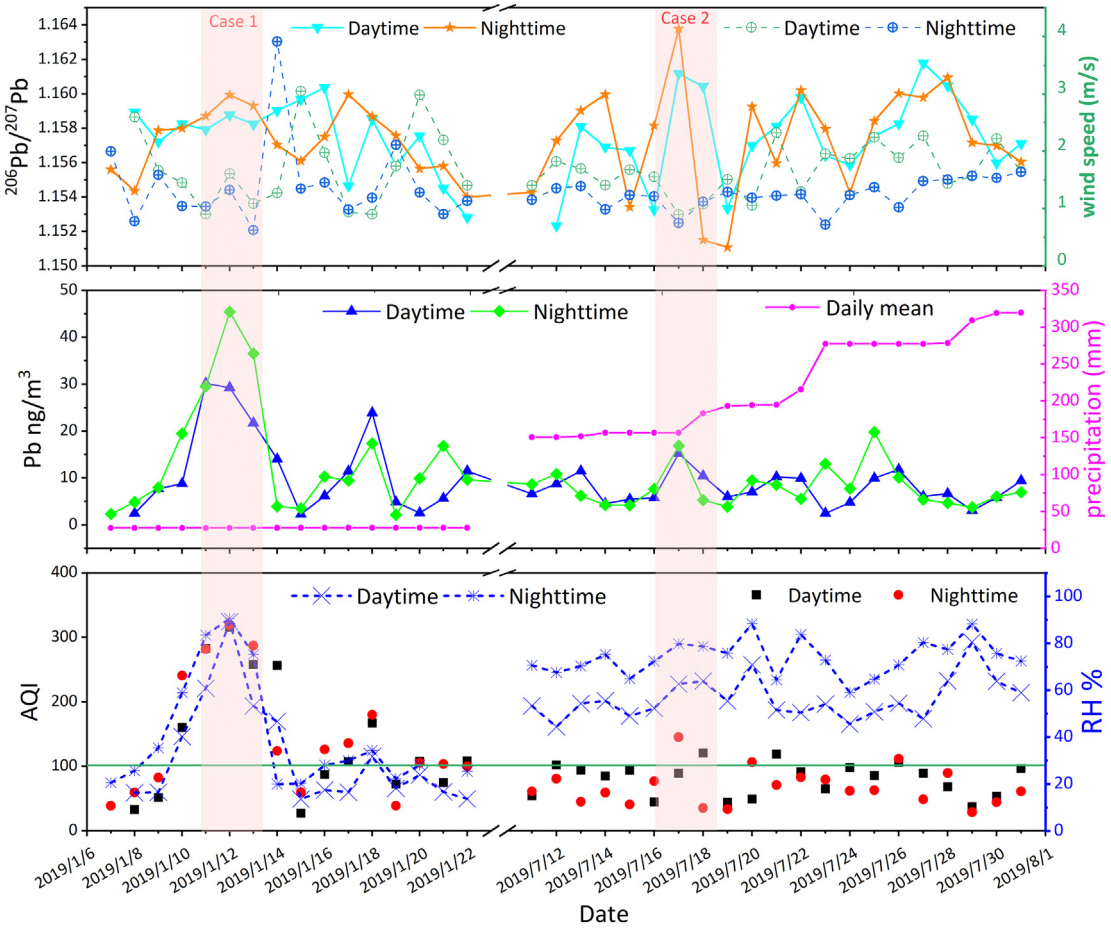

Fig. 3. The time series of AQI, RH, precipitation, Pb concentration and corresponding $^{206}Pb/^{207}Pb$ ratio in PM_{10} (In the diurnal AQI curves, yellow and white areas divide polluted (AQI > 100) and clean episodes (AQI < 100), respectively.)

gradual decay. A consistent trend was also found for the $^{206}Pb/^{207}Pb$ ratios (discussions concerning the backward trajectory in Section 3.3). This phenomenon is typically attributed to the collective effects of meteorological and anthropogenic factors. High RH and low air temperature and wind speed were conducive to the accumulation of air pollutants in January. In contrast, high air temperature and wind speed benefitted their diffusion in July (DeGaetano and Doherty, 2004; Sun et al., 2006; Zheng et al., 2015).

The Pearson correlation coefficients between Pb concentration and RH in January and July were 0.87 and −0.12, respectively; they were −0.54 and −0.27 between Pb concentration and wind speed. In January, PM absorbed moisture and increased in size when the temperature was low and RH was high, making the heavier pollutant particles sink. Meanwhile, the stable atmospheric environment formed by low wind speed caused the pollutant particles to gather in the low air layer and hindered the diffusion of pollutants. Low wind speeds are more conducive to the adsorption of Pb on small light particles suspended in the atmosphere. The adsorption of Pb was weaker on large particles, which are easily removed by gravity via dry deposition (Kim et al., 1997). Although the Pb concentration in PM_{10} was strongly correlated with meteorological parameters (RH and wind speed), anthropogenic emissions had a greater influence on the Pb concentration regarding seasonal variation.

The low correlation between Pb concentrations and meteorological factors in July indicated that emission sources mainly controlled Pb concentrations during this season. However, precipitation was also a potential factor affecting the variation in the Pb concentration in aerosols. During the summer precipitation period, atmospheric Pb loaded in the PM was removed by wet deposition, and the particles washed down by rainfall formed part of the urban dust. We found that the $^{206}Pb/^{207}Pb$ ratio in PM_{10} also changed significantly during the rainfall events. After a rainfall event, dust from roads and soil input some Pb into the atmosphere (Tao et al., 2021), with high summer temperatures and strong winds.

3.2. Pb sources in PM_{10} samples

Previous studies have successfully used the Pb isotopic method to identify the sources of atmospheric Pb pollution (Ewing et al., 2010; Zhao et al., 2015; Tao et al., 2021). Pb isotopic compositions were measured in source samples from local emissions. As shown in Fig. 4, vehicle emissions (from gasoline and diesel) and iron and steel plant B fly ash samples from the local emission sources in Tianjin were lower (mean $^{206}Pb/^{207}Pb$ = 1.49775) and higher (mean $^{206}Pb/^{207}Pb$ = 1.17135) than radiogenic Pb (here defined as containing more ^{206}Pb), respectively. The Pb isotopic ratios for most PM_{10} samples overlapped with coal combustion fly ash, vehicle emissions, and industrial activities (Fig. 4). They were clustered within a mixed region among multiple emission sources. The Pb isotopic data of the source samples in this study are listed in Table S5 and summarised in Table 1.

As shown in Fig. 5, $^{206}Pb/^{207}Pb$ and $^{208}Pb/^{206}Pb$ ratios of local Pb emission exhibited a strong linear correlation (R^2 = 0.92), and the fitting line was referred to “Local Pb emission sources mixed line (Tianjin)”. The PM_{10} samples were distributed on both sides of the mixed line. The winter samples were dispersive and highly concentrated in summer, which indicates that the Pb load in the winter samples may have contributed to regional transport in addition to the influence of local emission sources. Pb produced in the troposphere by human and industrial activities was mainly present as submicron particles. These Pb-containing aerosols contribute atmospheric Pb to other regions through long-range transport via atmospheric circulation. Therefore, the PM_{10} load, Pb, may originate from

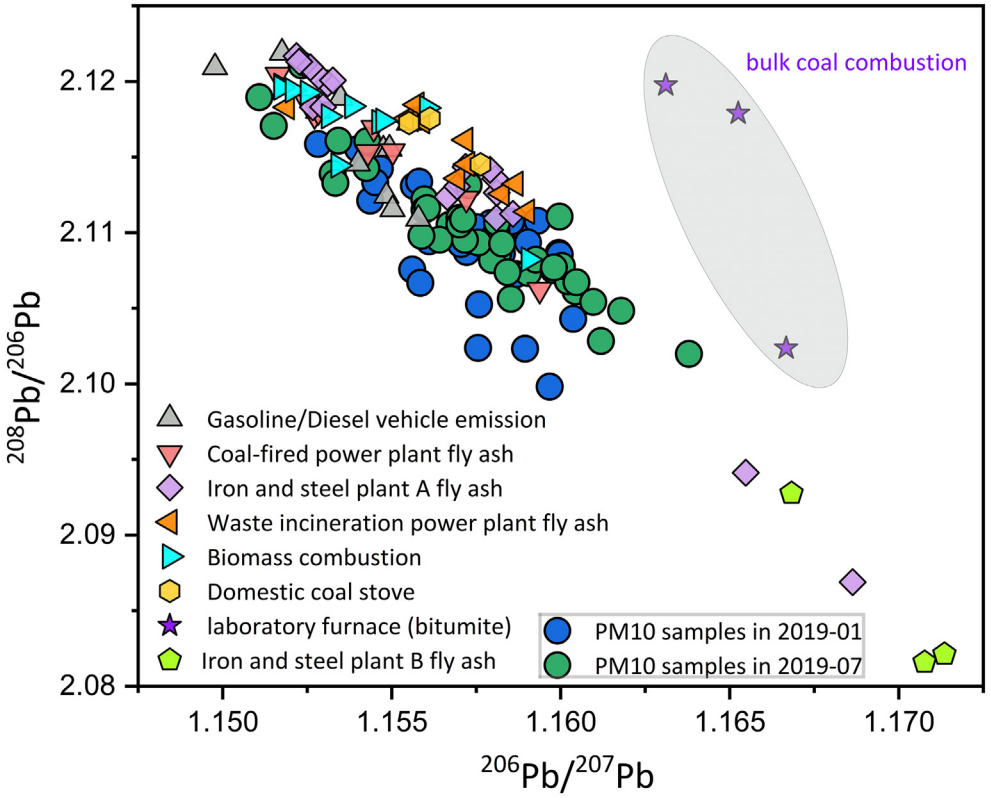

Fig. 4. $^{206}Pb/^{207}Pb$ vs. $^{208}Pb/^{206}Pb$ of PM_{10} samples and emission sources samples.

multiple local sources, significantly affected by coal combustion, steel plants, and vehicle emissions in Tianjin.

3.2.1. Coal combustion

Coal combustion is the largest potential source of anthropogenic Pb in Tianjin. In 2017, 1.83 billion tons of coal were used in coal-fired power plants in China, which accounted for 47.5 % of the total coal consumption (Table S6, National Bureau of Statistic of China, 2018). Coal combustion fly ash (simply the solid products of coal combustion) had a relatively low proportion median source contribution, which was the Pb isotopic composition of coal combustion fly ash ($^{206}Pb/^{207}Pb$ = 1.15163–1.15938). The coal originated from similar sources because of minimal fractionation during combustion (Kousehlar and Widom, 2020), and was likely similar to North China coal which comprised the least radiogenic Pb ($^{206}Pb/^{207}Pb$ < 1.17, Bi et al., 2017).

In addition to coal consumption for electricity and thermal systems, residents in most rural areas and parts of cities use raw coal for cooking and heating (WHO, 2014). The challenge of bulk coal consumption in suburban and rural areas has often been ignored because of the significant differences between the environmental targets of energy utilisation in urban and suburban areas (Chen et al., 2015; Li et al., 2021a, 2021b). A clear difference was observed in the Pb isotopic composition of coal-fired power plant (mean, 1.15428 ± 0.0024) and bulk coal burnt in the laboratory furnace (mean, 1.16501 ± 0.0018), which may be due to the different periods of coal formation (or the different geotectonic settings of the coal mines) for raw coal-fired power plants and bulk coal using in the laboratory. Another possible reason could be the combination of Pb during and after coal formation and heterogeneous Th/U distributions, which affected the Pb isotopic compositions of the two raw coals (Díaz-Somoano et al., 2007; Bi et al., 2017).

3.2.2. Iron and steel smelting plant

The Pb isotopic compositions of the steel-smelting samples from the two major plants (based on metallurgy) are presented in Table S5. Steelmaking processes contribute to the majority of heavy metal emissions (Wang et al.,

Table 1
The Pb isotopic composition of collecting the PM_{10} and Pb emission sources samples.

Sampling type		Sampling number	Pb concentration (μg m^{-3})	$^{206}Pb/^{207}Pb$				$^{208}Pb/^{206}Pb$			
				Mean	SD	Maximum	Minimum	Mean	SD	Maximum	Minimum
PM_{10} (January 2019)		31	13.3 ± 11.2[a]	1.15737	0.0020	1.16037	1.15282	2.10928	0.0037	2.11587	2.09982
PM_{10} (July 2019)		41	7.9 ± 3.8[a]	1.15743	0.0029	1.16379	1.14204	2.1101	0.0040	2.13718	2.10198
Coal-fired power plant fly ash		10	0.44 ± 0.36	1.15428	0.0024	1.15938	1.15163	2.11593	0.0041	2.12045	2.10624
Domestic coal combustion fly ash	Burning in rural stoves	3	2891 ± 3861	1.16501	0.0018	1.16667	1.16311	2.11334	0.009	2.11976	2.10237
	Burning in the lab's furnace	3	4.6 ± 4.2	1.15642	0.0011	1.15763	1.15551	2.11645	0.0017	2.11756	2.11452
Vehicle emission	Unleaded gasoline	6	4.5 ± 5.0	1.15340	0.0023	1.15579	1.14978	2.11676	0.0045	2.12189	2.11091
	Diesel	3	3.8 ± 2.1	1.15465	0.0006	1.15503	1.15400	2.11388	0.0021	2.11555	2.11455
Steel plant emission	Iron and steel plant A fly ash	20	5.4 ± 7.4	1.15611	0.0045	1.16863	1.15218	2.11433	0.0091	2.12167	2.08689
	Iron and steel plant B fly ash	3	16.4 ± 10.9	1.16965	0.0024	1.17135	1.16683	2.08549	0.0063	2.09276	2.08159
Cement plant fly ash		6	1.6 ± 1.2	1.15581	0.0017	1.15824	1.15339	2.11632	0.0025	2.12000	2.11321
Waste incineration power plant fly ash		11	8.3 ± 7.8	1.15653	0.0019	1.15901	1.15190	2.11551	0.0025	2.11847	2.11139
Biomass combustion		11	360 ± 592	1.15390	0.0022	1.15901	1.15173	2.11724	0.0034	2.11971	2.10822

[a] unit ng m^{-3}.

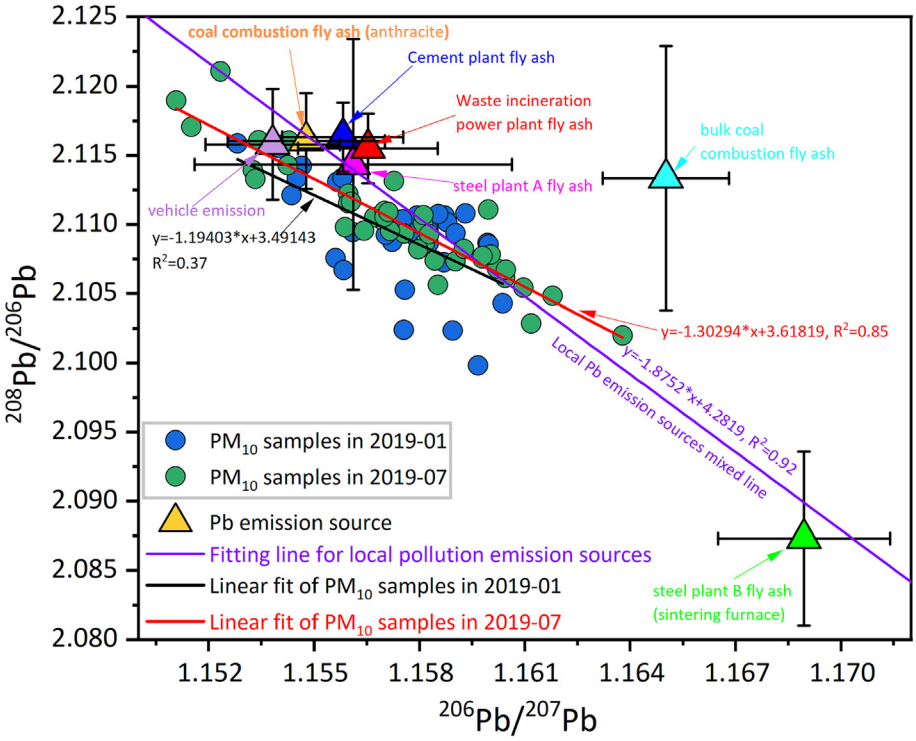

Fig. 5. $^{206}Pb/^{207}Pb$ vs. $^{208}Pb/^{206}Pb$ of PM_{10} samples and the average Pb isotopic ratios of each emission sources samples.

2016). The Bohai economic circle was identified as being among the top emission intensity regions, where iron and steel plants in northern China were potentially active regions (Wang et al., 2016; Dai et al., 2023). Therefore, Steel smelting plants were another important source of Pb emissions in Tianjin, providing high values of $^{206}Pb/^{207}Pb$. There was a significant difference in the Pb isotopic compositions of iron and steel smelting plants A and B, with higher $^{206}Pb/^{207}Pb$ in plant B than in plant A, but with a greater margin of error in plant A.

Compared with that in plant A, the relatively highly radiogenic Pb-containing ores were used for metallurgy in plant B. We collected samples from different processes and spot dust at plant A, such as sintering, pelletising, and blast-furnace hot stoves. In contrast, in plant B, we collected samples only from the end of the sintering machine. As a result, the PM collected from the different processes had different Pb isotopic signatures, resulting in a relatively large margin of error for the plant A samples. In addition, the Pb isotopic compositions of the fly ash collected from the different stages of the sintering furnace at plant A varied slightly, probably because of the different sources of coke dust input to the different processes.

3.2.3. Vehicle emission

The Pb isotopic compositions of diesel and gasoline presented a mixed characteristic similar to that of unleaded gasoline. Leaded petrol was banned in Tianjin in 1998. The isotope ratios in the aerosol showed a more "ore-like" composition (Koffman et al., 2022). $^{206}Pb/^{207}Pb$ ranged from 1.149 to 1.154 during 1994–1997 (Wang et al., 2006), whereas the aerosol Pb isotope ratios in January (mean, $^{206}Pb/^{207}Pb$ = 1.15737 ± 0.0020) and July (mean, $^{206}Pb/^{207}Pb$ = 1.15734 ± 0.0029) were significantly different from that before the phase-out of leaded gasoline. This finding suggests that the gasoline lead additive ban had a particularly important impact on Pb isotope compositions of aerosol samples in Tianjin. The Pb isotope ratios of vehicle emission were more "coal-like", consistent with previous studies; for example, it ranged from 1.158 to 1.161 in 1998–2001 (Wang et al., 2006) and 1.162 in 2017 (Deng et al., 2020). Our results indicate that some of the benefits of phased-out lead gasoline were transitory, whereas other industrial activities releasing Pb increased. Efforts have been made to decrease coal consumption and reduce the impact of atmospheric Pb in China. Thus, a significant decline in isotope ratios were present. Diesel is an important fuel used in ships. Thousands of ships sail in and out of Tianjin port, an international shipping hub in northern China. Studies have shown that while diesel contains more Pb than unleaded gasoline, the isotopic compositions of both fuel types are similar (Wang et al., 2003; Bi et al., 2017); therefore, ship exhaust is a potential source of atmospheric Pb pollution in Tianjin. Thus, the contribution of vehicular emissions to atmospheric Pb levels cannot be ignored.

3.2.4. Other secondary emission sources

The Pb isotope ratios of coal combustion were also close to those measured in secondary contributors, such as cement plants and waste incineration power plants. The cement plants and waste incineration power plants from which we collected samples added small amounts of coal as auxiliary fuel in some sections, such that the Pb isotopic compositions of some of the samples from these sources were similar to those of samples from coal-fired plants. For example, coal from Shanxi and Zhangjiakou was used in a cement plant in Tianjin, and a waste incineration power plant added 5 % pulverised coal as fuel to generate electricity together with domestic waste. This finding implies that coal is a stable pollution source that plays a significant role in atmospheric Pb pollution in Tianjin.

3.2.5. Estimation of Pb sources' contribution by the end-member model

Fig. 6a shows that the PM_{10} samples fall within the fields of China coal 1 ($^{206}Pb/^{207}Pb$ < 1.17, from North China), China fuel (diesel and unleaded gasoline), and China ore 2 (higher radiogenic Pb) corresponding to coal combustion, vehicle emissions, and steel plant emissions, respectively. We used a binary model developed from the two-end-member mixing line to calculate the relative contribution of coal combustion to the total Pb content in the PM_{10} samples (Monna et al., 1997). The expressions for the binary mixed model are shown in Eqs. (1) and (2).

$$Mix_{AB} = R_A \times f_A + R_B \times f_B \quad (1)$$

$$f_A + f_B = 1 \quad (2)$$

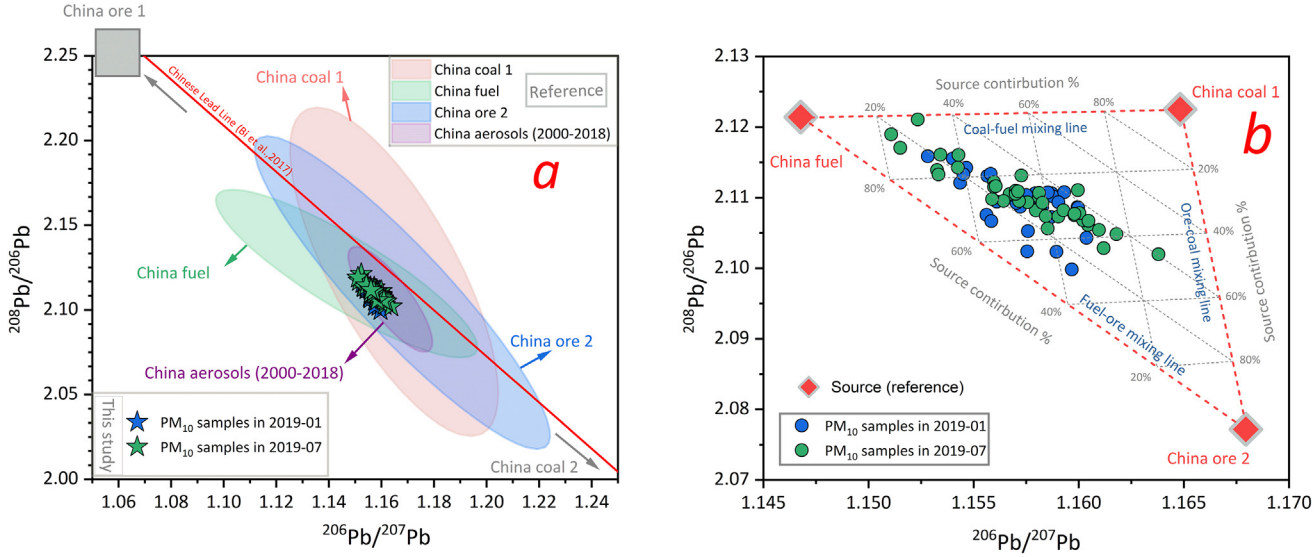

Fig. 6. (a)$^{206}Pb/^{207}Pb$ vs. $^{208}Pb/^{206}Pb$ of PM_{10} (this study) compared to potential pollution sources from reported (China coal 1 of the least radiogenic Pb and coal 2 higher radiogenic Pb represented originating North China and Southwest, respectively. China ore 1 and ore 2 represented originating the least radiogenic Pb higher radiogenic Pb, respectively). (b) The contribution of pollution end-member, with $^{206}Pb/^{207}Pb$ and $^{208}Pb/^{206}Pb$, is calculated using reported data from reference.

Mix_{AB} is the isotope ratio of a given mixture of end members A and B, which are different end-members. R_A and R_B are the corresponding isotope ratios of end-members A and B, respectively. For the selection of R_A and R_B, we used the data reported in the references, and detailed information about the selection of end-members is summarised in Test S3 and Table S7. f_A and f_B represent the fractions of the mixture that were contributed to by end-members A and B, respectively. As shown in Fig. 6d, the samples were mainly concentrated near the coal and fuel end members in the triangle (composed of China coal 1, China fuel, and China ore 2). Depending on the aerosol samples, we estimated the coal supply from approximately 20 % to 40 % of the PM_{10}-bound Pb at our sites in winter and summer. The main contributors to Pb emissions were coal combustion and ore smelting following the ban on lead in petrol.

3.3. Relative contribution of Pb sources for PM_{10} samples based on the MixSIAS model

Anthropogenic sources with a relatively broad range of compositions represent a mixture of coal combustion and vehicles and steel plant emissions. Therefore, we calculated the relative contribution of Pb from the main emission sources using the MixSIAS model. The Pb isotopic compositions of coal combustion, steel plants, and vehicle emissions were determined in this study. The total Pb concentration contribution (mean ± SD, ng m^{-3}) in PM_{10} for the three end-member sources and the percentages are summarised in Tables S8, and S9, respectively.

The time series of the relative contributions of the three sources are shown in Fig. 7a. No significant variation in the relative contribution of each source over time was present, and Pb sources from coal combustion were stable. However, minimal fluctuations in the relative contribution values of each source during the pollution period were present, which were influenced by local pollutants emissions and the meteorological conditions. During the polluted periods, the contribution of coal combustion was relatively high, and the contribution of coal combustion to Pb concentration reached 26.7 ng m^{-3} (2019-01-12-N). In Case 1, we observed a gradual increase and decrease in Pb concentrations with $^{206}Pb/^{207}Pb$ over time, with a consistent trend. Combining the six-day backward trajectory (Fig. S3: from January 10 to January 15), we found that the air masses carrying pollutants gradually converged towards the sampling site from the southwest during the beginning of the pollution event 1 (January 10). The pollution was the most severe on January 12, when the $^{206}Pb/^{207}Pb$ ratio of PM reached a maximum. Subsequently, the pollution gradually diminished as a clean air mass originated from the northwest. We speculated that PM carried from the southwest may have originated primarily from steel emission sources with a relatively high $^{206}Pb/^{207}Pb$ ratio. Its relative contribution progressively increased and then decreased during this pollution event, reaching 30.6 % (2019-01-12-N). In pollution event Case 2, we found an increased and then decreased variation in Pb concentration and $^{206}Pb/^{207}Pb$ over time (16th to 18th, 17th to 18th July). Combining the six-day backward trajectory (Fig. S4: from 15th to 20th January), we found that the southeast air masses carried a lower $^{206}Pb/^{207}Pb$ ratio, which probably originated from unleaded gasoline and/or diesel emissions, when the $^{206}Pb/^{207}Pb$ ratio of PM reached a minimum on July 18 (2019-07-18-D). The two pollution events were mainly owing to decreasing wind speeds and increasing RH (Fig. 3), which made it easier for pollutants to accumulate in urban. Thus, majority of locally anthropogenic emissions of pollutants are difficult to diffuse over a short period. The results from the MixSIAS model also illustrate that the sources of vehicle emissions increased. Our results show that the contribution of Pb sources to the collected PM varied significantly between air masses carrying different PM sources during periods of pollution, depending on the complex interactions among meteorological conditions, pollution sources, and atmospheric chemical processes (Wang et al., 2014; Wei et al., 2019; Li et al., 2021a, 2021b).

Moreover, the contribution of steel plant source emissions increased by 6.6 %. In contrast, the percentage of coal combustion in PM_{10} decreased by 9.7 % in July (Fig. 7b). This seasonal difference may be due to the increase in coal consumption for heating, one of the most basic living requirements in northern China during winter. Nevertheless, coal combustion remains an important anthropogenic source of Pb aerosols in Tianjin. Therefore, further energy structure adjustment should be accelerated to reduce pollutant emissions. Furthermore, the government should continuously promote the deep treatment or transformation of coal-fired units, hasten the clean replacement of raw materials and fuel coal in industrial kilns and incinerators, and promote the conversion and integration of coal-fired boilers.

4. Conclusion

In this study, we investigated the sources and concentrations of atmospheric Pb in Tianjin. The PM_{10}-bond Pb originated from coal combustion and vehicle and steel plant emissions, mainly from local Pb emission

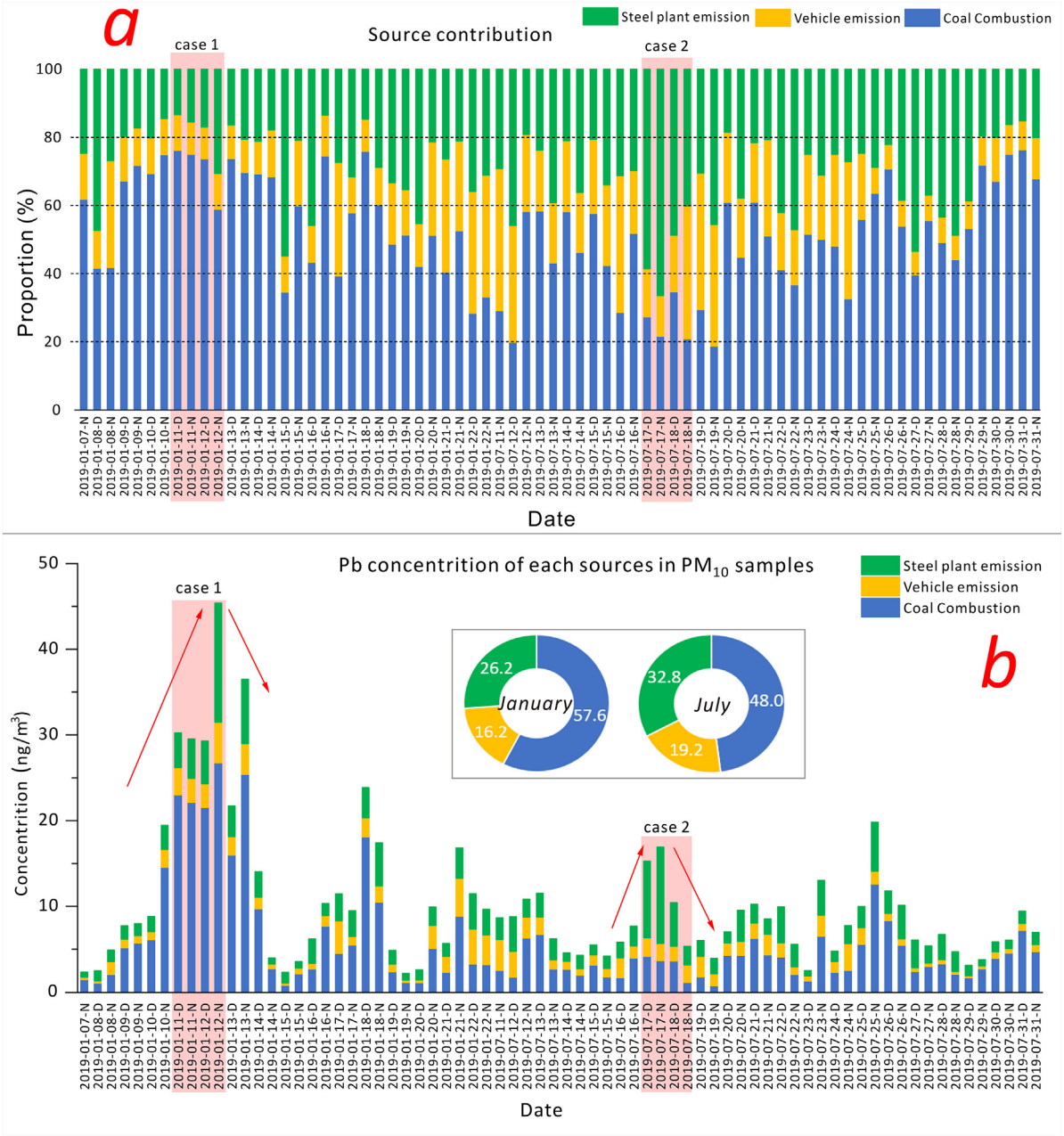

Fig. 7. (a) The contribution percentage of coal combustion, vehicle emission and steel plant emission sources for Pb in PM_{10}. (b) The contributed concentration of coal combustion, vehicle and steel plant sources emission for Pb in PM_{10}.

sources in Tianjin. The PM_{10}-bond Pb in January was influenced by regional transportation and local sources. The contribution of coal combustion to the total Pb in the aerosol at 57.6 ± 14.9 % was dominant in the winter based on the MixSIAS model. Our results indicate that some of the benefits of phased-out lead gasoline have been transitory, whereas other industrial activities releasing Pb have increased. The results of this study provide data to better understand the compositional characteristics and sources of atmospheric Pb isotopes during periods of atmospheric pollution and clean up, as well as the Pb isotope source spectra of major Pb emission sources in the BTH region.

CRediT authorship contribution statement

Wen-Jing Dai: Data curation, Investigation, Writing-Original Draft.
Yu-Cong Fu: Investigation.
Xiao-Dong Li: Review, Validation.
Shi-Yuan Ding: Review.
Qin-Kai Li: Collecting samples.
Zhi-Qi Zhao: Resources, Review, Methodology, Validation.

Data availability

Data will be made available on request.

Declaration of competing interest

We declare that we have no conflicts of interest to this work. We declare that we do not have any commercial or associative interest that represents a conflict of interest in connection with the work submitted. The manuscript entitled, "Identification and contribution of potential sources to atmospheric

lead pollution in a typical megacity: Insights from isotope analysis and the Bayesian mixing model" by Wen-Jing Dai, Yu-Cong Fu, Xiao-Dong Li, Shi-Yuan Ding, Qin-Kai Li, Zhi-Qi Zhao.

Acknowledgements

We would like to sincerely thank Dr. Jun-Wen Zhang, Dr. Zheng-Hua Tao, Dr. Hao Xiao for their valuable suggestions and comments on the revision of this paper. Project supported by the National Key Research and Development Program of China (Grant No. 2017YFC0212701), the Natural Science Foundation of Shaanxi Province (Nos. 2022JZ-19 and 2022JQ-229), the Natural Science Foundation of Tianjin (Grant No. 22JCQNJC00700).

Appendix A. Supplementary data

Supplementary data to this article can be found online at https://doi.org/10.1016/j.scitotenv.2023.164567.

References

Bi, X.Y., Li, Z.G., Wang, S.X., Zhang, L., Xu, R., Liu, J.L., Yang, H.M., Guo, M.Z., 2017. Lead isotopic compositions of selected coals, Pb/Zn ores and fuels in China and the application for source tracing. Environ. Sci. Technol. 51, 13502–13508.

Charlesworth, S., Everett, M., McCarthy, R., Ordóñez, A., de Miguel, E., 2003. A comparative study of heavy metal concentration and distribution in deposited street dusts in a large and a small urban area: Birmingham and Coventry, West Midlands, UK. Environ. Int. 29, 563–573.

Chen, J., Tan, M., Li, Y., Zhang, Y., Lu, W., Tong, Y., Zhang, G., Li, Y., 2005. A lead isotope record of Shanghai atmospheric lead emissions in total suspended particles during the period of phasing out of leaded gasoline. Atmos. Environ. 39, 1245–1253.

Chen, J., Tan, M., Li, Y., Zheng, J., Zhang, Y., Shan, Z., Zhang, G., Li, Y., 2008. Characteristics of trace elements and lead isotope ratios in $PM_{2.5}$ from four sites in Shanghai. J. Hazard. Mater. 156, 36–43.

Chen, P., Bi, X., Zhang, J., Wu, J., Feng, Y., 2015. Assessment of heavy metal pollution characteristics and human health risk of exposure to ambient $PM_{2.5}$ in Tianjin, China. Particuology 20, 104–109.

Chen, H., Yan, Y.L., Hu, D.M., Peng, L., Wang, C., 2023. High contribution of vehicular exhaust and coal combustion to $PM_{2.5}$-bound Pb pollution in an industrial city in North China: an insight from isotope. Atmos. Environ. 294, 119503.

Child, A.W., Moore, B.C., Vervoort, J.D., Beutel, M.W., 2018. Bioavailability and uptake of smelter emissions in freshwater zooplankton in northeastern Washington, USA lakes using pb isotope analysis and trace metal concentrations. Environ. Pollut. 238, 348–358.

Dai, Q.L., Chen, J.J., Wang, X.H., Dai, T.J., Tian, T.Z., Bi, X.H., Shi, G.L., Wu, J.H., Liu, B.S., Zhang, Y.F., Yan, B.Z., Kinney, P.L., Feng, Y.C., Hopke, P.K., 2023. Trends of source apportioned PM2.5 in Tianjin over 2013–2019: impacts of clean air actions. Environ. Pollut. 325, 121344.

DeGaetano, A.T., Doherty, O.M., 2004. Temporal, spatial and meteorological variations in hourly PM2.5 concentration extremes in New York City. Atmos. Environ. 38 (11), 1547–1558.

Deng, L., Bi, C.J., Jia, J.P., Zeng, Y.S., Chen, Z.L., 2020. Effects of heating activities in winter on characteristics of PM2.5-bound Pb, Cd and lead isotopes in cities of China. J. Clean. Prod. 265, 121826.

Díaz-Somoano, M., Suárez-Ruiz, I., Alonso, J.I.G., Encinar, J.R., López-Antón, M.A., Martínez-Tarazona, M.R., 2007. Lead isotope ratios in Spanish coals of different characteristics and origin. Int. J. Coal Geol. 71, 28–36.

Dietrich, M., Krekeler, M.P.S., Kousehlar, M., Widom, E., 2021. Quantification of Pb pollution sources in complex urban environments through a multi-source isotope mixing model based on Pb isotopes in lichens and road sediment. Environ. Pollut. 288, 117815.

Ewing, S.A., Christensen, J.N., Brown, S.T., Vancuren, R.A., Cliff, S.S., De Paolo, D.J., 2010. Pb isotopes as an indicator of the asian contribution to particulate air pollution in urban California. Environ. Sci. Technol. 44 (23), 8911–8916.

Fang, W., Delapp, R.C., Kosson, D.S., van der Sloot, H.A., Liu, J., 2017. Release of heavy metals during long-term land application of sewage sludge compost: percolation leaching tests with repeated additions of compost. Chemosphere. 169, 271–280.

Fry, K.L., Wheeler, C.A., Gillings, M.M., Flegal, A.R., Taylor, M.P., 2020. Anthropogenic contamination of residential environments from smelter As, Cu and Pb emissions: implications for human health. Environ. Pollut. 262, 114235.

Gao, Y., Guo, X., Li, C., Ding, H., Tang, L., Ji, H., 2015. Characteristics of $PM_{2.5}$ in Miyun, the northeastern suburb of Beijing: chemical composition and evaluation of health risk. Environ. Sci. Pollut. Res. Int. 22, 16688–16699.

Gao, P.P., Xue, P.Y., Dong, J.W., Zhang, X.M., Sun, H.X., Geng, L.P., Luo, S.X., Zhao, J.J., Liu, W.J., 2021. Contribution of $PM_{2.5}$-Pb in atmospheric fallout to Pb accumulation in Chinese cabbage leaves via stomata. J. Hazard. Mater. 407, 124356.

Gioia, S.M.C.L., Pimentel, M.M., Tessler, M., Dantas, E.L., Campos, J.E.G., Guimarães, E.M., Maruoka, M.T.S., Nascimento, E.L.C., 2006. Sources of anthropogenic lead in sediments from an artificial lake in Brasíliaecentral Brazil. Sci. Total Environ. 356, 125–142.

Graney, J.R., Edgerton, E.S., Landis, M.S., 2019. Using Pb isotope ratios of particulate matter and epiphytic lichens from the Athabasca Oil Sands Region in Alberta, Canada to quantify local, regional, and global Pb source contributions. Sci. Total Environ. 654, 1293–1304.

Harlavan, Y., Shirav, M., Ilani, S., Halicz, L., Yoffe, O., 2021. The fate of anthropogenic Pb in soils; years after Pb terminated as a fuel additive; Northern Israel. Environ. Pollut. 271, 116319.

Hinrichs, J., Dellwig, O., Brumsack, H.J., 2002. Lead in sediments and suspended particulate matter of the German Bight: natural versus anthropogenic origin. Appl. Geochem. 17, 621–632.

Hu, J., Chen, W.P., Zhao, Z.Q., Lu, R., Cui, M., Dai, W.J., Ma, W.M., Feng, X., Wan, X.M., Wang, N., 2022. Source tracing of potentially toxic elements in soils around a typical coking plant in an industrial area in northern China. Sci. Total Environ. 807, 151091.

Huang, H., Jiang, Y., Xu, X., Cao, X., 2018. In vitro bioaccessibility and health risk assessment of heavy metals in atmospheric particulate matters from three different functional areas of Shanghai, China. Sci. Total Environ. 610-611, 546–554.

Kayee, J., Sompongchaiyakul, P., Sanwlani, N., Bureekul, S., Wang, X.F., Das, R., 2020. Metal concentrations and source apportionment of PM2.5 in Chiang Rai and Bangkok, Thailand during a biomass burning season. ACS Earth Space Chem. 4, 1213–1226.

Kim, K.H., Kim, D.S., Lee, T.J., 1997. The temporal variabilities in the concentrations of airborne lead and its relationship to aerosol behavior. Atmos. Environ. 31 (20), 3449–3458.

Koffman, P., Saylor, P., Zhong, R.J., Sethares, L., Yoder, M.F., Hanthven, T., Cai, Y., Bolge, L., Longman, J., Goldstein, S.L., Osterberg, E.C., 2022. Provenance of anthropogenic Pb and atmospheric dust to Northwestern North America. Environ. Sci. Technol. 56 (18), 13107–13118.

Kousehlar, M., Widom, E., 2020. Identifying the sources of air pollution in an urbanindustrial setting by lichen biomonitoring-a multi-tracer approach. Appl. Geochem. 121, 104695.

Lee, S., Han, C., Shin, D., Choi, K., Hur, S.D., Jun, S.J., Kim, Y.T., Byun, D.S., Hong, S., 2017. Characteristics of elemental and Pb isotopic compositions in aerosols ($PM_{10\text{-}2.5}$) at the Ieodo Ocean Research Station in the East China Sea. Environ. Pollut. 231, 154–164.

Li, Q., Cheng, H., Zhou, T., Lin, C., Guo, S., 2012. The estimated atmospheric lead emissions in China, 1990–2009. Atmos. Environ. 60, 1–8.

Li, H., Qian, X., Wang, Q., 2013. Heavy metals in atmospheric particulate matter: a comprehensive understanding is needed for monitoring and risk mitigation. Environ. Sci. Technol. 47, 13210–13211.

Li, X., Bi, X., Li, Z., Zhang, L., Fu, X., 2019. Atmospheric lead emissions from coal-fired power plants with different boilers and APCDs in Guizhou, Southwest China. Energy Fuel 33, 10561–10569.

Li, W.G., Duan, F.K., Zhao, Q., Song, W.W., Chen, Y., Wang, X.Y., Cheng, Y., Wang, X.Y., Li, L., He, K.B., 2021a. Investigating the effect of sources and meteorological conditions on wintertime haze formation in Northeast China: a case study in Harbin. Sci. Total Environ. 801, 149631.

Li, B., Sun, Y., Zheng, W., Zhang, H., Jurasz, J., Du, T., Wang, Y., 2021b. Evaluating the role of clean heating technologies in rural areas in improving the air quality. Appl. Energy 289, 116693.

Liu, J.K., Han, G.L., 2021. Tracing riverine particulate black carbon sources in Xijiang River basin: insight from stable isotopic composition and Bayesian mixing model. Water Res. 194, 116932.

Marx, S.K., Rashid, S., Stromsoe, N., 2016. Global-scale patterns in anthropogenic pb contamination reconstructed from natural archives. Environ. Pollut. 213, 283–298.

Monna, F., Lancelot, J., Croudace, I.W., Cundy, A.B., Lewis, J.T., 1997. Pb isotopic composition of airborne particulate material from France and the southern United Kingdom: implications for Pb pollution sources in urban areas. Environ. Sci. Technol. 31 (8), 2277–2286.

Moore, J.W., Semmens, B.X., 2008. Incorporating uncertainty and prior information into stable isotope mixing models. Ecol. Lett. 11 (5), 470–480.

Outridge, P.M., Hermanson, M.H., Lockhart, W.L., 2002. Regional variations in atmospheric deposition and sources of anthropogenic lead in lake sediments across the Canadian Arctic. Geochem. Cosmochim. Acta 66 (20), 0–3531.

Peng, B., Chen, H.S., Fang, X.H., Xie, S.R., Wu, S.C., Jiang, C.X., Dai, Y., 2022a. Distribution of Pb isotopes in different chemical fractions in bed sediments from lower reaches of the Xiangjiang River, Hunan province of China. Sci. Total Environ. 829, 154394.

Peng, B., Juhaz, A., Fang, X.H., Jiang, C.X., Wu, S.C., Li, X.M., Xie, S.R., Dai, Y., 2022b. Lead isotopic fingerprinting as a tracer to identify the sources of heavy metals in sediments from the Four Rivers' inlets to Dongting Lake, China. Catena 219, 106594.

Pérez-Rodríguez, M., Silva-Sánchez, N., Kylander, M.E., Bindler, R., Mighall, T.M., Schofield, J.E., 2018. Industrial-era lead and mercury contamination in southern Greenland implicates North American sources. Sci. Total Environ. 613, 919–930.

Rauch, J.N., Pacyna, J.M., 2009. Earth's global Ag, Al, Cr, Cu, Fe, Ni, Pb, and Zn cycles. Glob. Biogeochem. Cycles 23 (2), GB2001.

Stock, B.C., Jackson, A.L., Ward, E.J., Parnell, A.C., Phillips, D.L., Semmens, B.X., 2018. Analyzing mixing systems using a new generation of Bayesian tracer mixing models. PeerJ 6, 5096.

Stock, B. C, Semmens, B. X, 2016. Unifying error structures in commonly used biotracer mixing models. Ecology 97 (10), 2562–2569.

Sun, Y.L., Zhuang, G.S., Zhang, W.J., Wang, Y., Zhuang, Y.H., 2006. Characteristics and sources of lead pollution after phasing out leaded gasoline in Beijing. Atmos. Environ. 40 (16), 2973–2985.

Tao, Z., Guo, Q., Wei, R., Dong, X., Han, X., Guo, Z., 2021. Atmospheric lead pollution in a typical megacity: evidence from lead isotopes. Sci. Total Environ. 778, 145810.

Tian, H., Zhu, C., Gao, J., Cheng, K., Hao, J., Wang, K., 2015. Quantitative assessment of atmospheric emissions of toxic heavy metals from anthropogenic sources in China: historical trend, spatial distribution, uncertainties, and control policies. Atmos. Chem. Phys. 15 (17), 10127–10147.

Todt, W., Cli, R.A., Hanser, A., Hofmann, A.W., 1993. Re-calibration of NBS lead standards using a ^{202}Pb + ^{205}Pb double spike. Terra Nova 5 (Abstr. suppl. 1), 396.

Wan, D., Yang, H., Jin, Z., Xue, B., Song, L., Mao, X., Yang, J., 2020. Spatiotemporal trends of atmospheric Pb over the last century across inland China. Sci. Total Environ. 729, 138399.

Wang, Y.F., Huang, K.L., Li, C.T., Mi, H.H., Luo, J.H., Tsai, P.J., 2003. Emissions of fuel metals content from a diesel vehicle engine. Atmos. Environ. 37, 4637–4643.

Wang, W., Liu, X., Zhao, L., Guo, D., Tian, X., Adams, F., 2006. Effectiveness of leaded petrol phase-out in Tianjin, China based on the aerosol lead concentration and isotope abundance ratio. Sci. Total Environ. 364, 175–187.

Wang, Y., Li, L., Chen, C.H., Huang, C., Huang, H.Y., Feng, J.L., Wang, S.X., Wang, H.L., Zhang, G., Zhou, M., Cheng, P., Wu, M.H., Sheng, G.Y., Fu, J.M., Hu, Y., Russell, A.G., Wumaer, A., 2014. Source apportionment of fine particulate matter during autumn haze episodes in Shanghai, China. J. Geophys. Res. Atmos. 119, 1903–1914.

Wang, K., Tian, H.Z., Hua, S.B., Zhu, C.Y., Gao, J.J., Xue, Y.F., Hao, J.M., Wang, Y., Zhou, J.R., 2016. A comprehensive emission inventory of multiple air pollutants from iron and steel industry in China: temporal trends and spatial variation characteristics. Sci. Total Environ. 559, 7–14.

Wei, X.Y., Liu, M., Yang, J., Du, W.N., Sun, X., Huang, Y.P., Zhang, X., Khalil, S.K., Luo, D.M., Zhou, Y.D., 2019. Characterization of PM2.5-bound PAHs and carbonaceous aerosols during three-month severe haze episode in Shanghai, China: chemical composition, source apportionment and long-range transportation. Atmos. Environ. 203, 1–9.

WHO, 2014. WHO Guidelines for Indoor Air Quality: Household Fuel Combustion. World Health Organization, Geneva.

Widory, D., Roy, S., Le Moullec, Y., Goupil, G., Cocherie, A., Guerrot, C., 2004. The origin of atmospheric particles in Paris: a view through carbon and lead isotopes. Atmos. Environ. 38, 953–961.

Wu, Y., Lou, J., Sun, X., Ma, L.Q., Wang, J., Li, M., Sun, H., Li, H., Huang, L., 2020. Linking elevated blood lead level in urban school-aged children with bioaccessible lead in neighborhood soil. Environ. Pollut. 261, 114093.

Xu, H., Sonke, J.E., Guinot, B., Fu, X., Sun, R., Lanzanova, A., Candaudap, F., Shen, Z., Cao, J., 2017. Seasonal and annual variations in atmospheric Hg and Pb isotopes in Xi'an, China. Environ. Sci. Technol. 51 (7), 3759–3766.

Zhao, Z.Q., Zhang, W., Li, X.D., Yang, Z., Zheng, H.Y., Ding, H., Wang, Q.L., Xiao, J., Fu, P.Q., 2015. Atmospheric lead in urban Guiyang, Southwest China: isotopic source signatures. Atmos. Environ. 115, 163–169.

Zheng, G.J., Duan, F.K., Su, H., Ma, Y.L., Cheng, Y., Zheng, B., Zhang, Q., Huang, T., Kimoto, T., Chang, D., Pöschl, U., Cheng, Y.F., He, K.B., 2015. Exploring the severe winter haze in Beijing: the impact of synoptic weather, regional transport and heterogeneous reactions. Atmos. Chem. Phys. 15 (6), 2969–2983.